A Simple and Efficient Method of Moments Solution Procedure for Solving Time-Domain Integral Equation—Application to Wire-Grid Model of Perfect Conducting Objects

Sadasiva Rao 🆔, *Fellow, IEEE*

Abstract—In this paper, a straightforward method of moments procedure to solve the time-domain integral equation is presented and applied to a wire-grid model of an arbitrarily shaped conducting body. The conducting body is illuminated by a Gaussian plane wave. Contrary to all the available time-domain algorithms, this procedure does not involve marching in time thus eliminating error accumulation, a major source for late-time instability problem. The procedure presented in this paper is conceptually simple, numerically efficient, and handles multiple excitations in a trivial manner, all the while remaining stable. The numerical procedure utilizes pulse functions for space variable and time-shifted Gaussian functions for time variable, respectively. Furthermore, the numerical procedure adopts Galerkin method of solution implying the usage of same time and space functions for both expansion and testing. The numerical results obtained in the time domain are validated by comparing with the data obtained from the frequency domain solution at several frequencies and performing inverse discrete Fourier transform.

Index Terms—Electromagnetic scattering, method of moments, time domain analysis.

I. INTRODUCTION

UNTIL recently, a time-stepping process, popularly known as the Marching-on-in-Time (MOT) method [1], has been the preferred technique for solving the numerical solution of Time-Domain Integral Equation (TDIE) for electromagnetic field problems. The main advantage of the MOT method is that, when used as an explicit scheme, it requires no matrix inversion, a computationally intensive step in any numerical algorithm [1]. Unfortunately, the MOT procedure is prone to late-time instabilities. The primary source of instability seems to be the method itself where the accumulation of error occurs at each time step. Over the last 50 years, there have been several proposed remedies to overcome this problem [2]–[20]. However, most of the proposed remedies only try to arrest the instabilities, successful only for simple problems, and invariably fail for complex objects. Even the implicit schemes in time domain, which require

a matrix inversion, are vulnerable to the instability problem and hence are of little use to a practicing engineer.

Recently, a new type of algorithm was developed and applied to wire-grid models of arbitrary bodies to solve the TDIE using the conventional method of moments (MOM) solution procedure [21]. In the MOM numerical solution scheme, the arbitrary wire was divided into subdomains and the standard pulse functions were used to represent the space variable along the length of the wire. The time variable is approximated by a set of time-shifted Gaussian functions. Note that the time-shifted Gaussian functions represent entire domain functions and decay as time extends to infinity. As a result, the time-domain signature stays stable even at a late time. For testing purposes, point matching was used for both the space and time variables. Because of the conventional MOM procedure, the new method can handle multiple incident pulses, with varying frequency signature bands and directions of incidence, necessary for monostatic RCS calculations, with only a fractional additional cost as compared to a single incident field.

The most important point to be noted regarding the work presented in [21], and this paper, is the central idea is a departure from the time-marching methods of the previous 50 years. It should be noted that the problem is solved by developing a matrix equation over a fixed time interval and space domain utilizing the standard MOM. Obviously, we have a lot of freedom in selecting basis and testing functions for the MOM solution which eventually dictates the structure of the MOM matrix and the accuracy of the solution. The final matrix equation can be solved in any suitable manner including inverting the matrix as done in [21]. Also, because of this fact, one can solve multiple right-hand sides unlike any previously available MOT methods. However, one disadvantage of this new procedure is the required inversion of large real matrix of dimension $P = M \times N$, where M and N represent the number of time functions and number of wire subdomains, respectively. Thus, the matrix P could be quite large even for moderately complex wire models.

In this paper, we alleviate this problem, i.e., storage and inversion of a large matrix, by redefining the Gaussian functions used for expressing the time variable in a controlled manner and adopting Galerkin procedure as described in the following sections. These modifications allow us to generate

Fig. 1. Arbitrary body modeled by wire grid.

Fig. 2. Wire segments connected to an ordinary node.
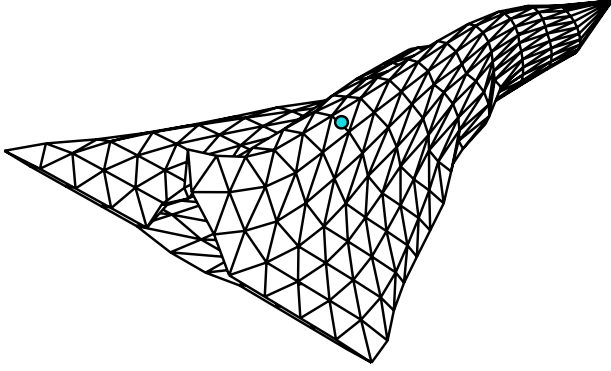
a blockwise lower triangular matrix, which is also blockwise Toeplitz, instead of a full matrix as in [21]. Further, the block-wise Toeplitz nature of the new matrix drastically reduces the storage also. Finally, the solution is obtained by a trivial process of back substitution resulting in an extremely efficient numerical procedure.

The new procedure offers several advantages and makes the algorithm computationally efficient. First of all, the MOM matrix of dimension P is a blockwise lower triangular matrix and, hence, easily solvable by back-substitution avoiding expensive matrix inversion. Next, the lower triangular matrix is also a block Toeplitz matrix with each block of dimension N. Thus, we need to compute only $P \times N$ elements compared to P^2 elements as in [21]. Since the matrix inversion step is eliminated, the new algorithm is very efficient and remains stable for very long solution times.

In the following sections, we present detailed mathematical steps, numerical solution procedure, and numerical results comparing with data obtained using the frequency domain MOMs (FD-MOM) solution plus IDFT procedure.

II. MATHEMATICAL FORMULATION

Consider an arbitrary shaped body, modeled as a wire-mesh as shown in Fig. 1, illuminated by a time-domain pulse. Following the mathematical procedure presented in [1], the TDIE may be written as

$$\left[\frac{\partial^2 \boldsymbol{A}}{\partial t^2} + \nabla \Psi \right]_{\tan} = \left[\frac{\partial \boldsymbol{E}^i}{\partial t} \right]_{\tan} \tag{1}$$

where

$$\boldsymbol{A}(t, \boldsymbol{r}) = \mu \int_\ell \frac{\hat{s}' I(t - R/c, \boldsymbol{r}')}{4\pi R} \, d\ell' \tag{2}$$

$$\Psi(t, \boldsymbol{r}) = \frac{-1}{\epsilon} \int_\ell \frac{\partial I(t - R/c, \boldsymbol{r}')/\partial \ell}{4\pi R} \, d\ell' \tag{3}$$

$$\text{and} \quad R = \sqrt{|\boldsymbol{r} - \boldsymbol{r}'| + a^2}. \tag{4}$$

In (1)–(4),

$\hat{s} \rightarrow$ Unit vector along the wire axis.
$I \rightarrow$ Induced current.
$\boldsymbol{r} \rightarrow$ Observation point on the body.
$\boldsymbol{r}' \rightarrow$ Source point on the body.

$\boldsymbol{E}^i \rightarrow$ Incident electric field.
$\mu \rightarrow$ permeability of the surrounding space.
$\epsilon \rightarrow$ permittivity of the surrounding space.
$a \rightarrow$ radius of the wire.

Next, we consider the solution of (1) using the MOM.

III. MOM SOLUTION PROCEDURE

First of all, we note that the wire mesh consists of several electrically short wires, referred to as wire segments, mutually attached to each other to approximate the given body. The common point where several wire segments are attached is known as a *node*. If only one segment is attached to a node, then that node is referred to as a *boundary node* and removed from the solution scheme. When only two wires are attached to a given node, the node is referred to as an *ordinary node* and one unknown is associated with this node as shown in Fig. 2. Further, if more than two wire segments are attached to a given node, then we have a *junction node* and the number of unknowns associated with this junction node is one less than the total number of wires connected to this node. We note that the junction node can be easily handled in an identical manner as an ordinary node as presented in [1] and [21].

Let us consider an ordinary node as shown in Fig. 2. Let the position vector $\boldsymbol{r}_n$, defined with respect to the global coordinate origin $\bigcirc$, represent the nth node. Two-wire segments $S_n^\pm$, with radii $a_n^\pm$, are connected to this node and the induced current is arbitrarily chosen as flowing from S_n^- to S_n^+.

Next, for numerical purposes, let us define the upper limit on the time variable $t = T$, where T represents the time when the incident pulse becomes negligible. Then, we divide the time axis $0 \rightarrow T$ into M uniform time intervals given by Δt and denote $t_m = m\Delta t$ for $m = 1, 2, \ldots M$. We note that, initially, the MOM scheme is applied to a finite interval $0 \rightarrow T$. We also note that extending the time interval to later times is trivial as discussed later.

Now, we define the approximation to the induced current $I(t, \boldsymbol{r})$ as

$$I(t, \boldsymbol{r}) \approx \sum_{m=1}^{M} \sum_{n=1}^{N} I_{m,n} \, f_m(t) \, g_n(\boldsymbol{r}) \tag{5}$$

where

$$f_m(t) \equiv e^{-\left(\frac{t-m\,\Delta t}{\sigma}\right)^2} \quad 0 < t < \infty \tag{6}$$

and

$$g_n(\boldsymbol{r}) \equiv \begin{cases} 1, & \boldsymbol{r} \in (\boldsymbol{r}_{n-\frac{1}{2}}, \boldsymbol{r}_{n+\frac{1}{2}}) \\ 0, & \text{otherwise.} \end{cases} \tag{7}$$

In (6) and (7), σ represents the standard deviation of the Gaussian function and $\boldsymbol{r}_{n\pm\frac{1}{2}}$ represents the midpoint of segment $S_n^\pm$. Here, we note that the choice of σ is critical to obtain a blockwise Toeplitz moment matrix as discussed later.

Thus, for a complex body approximated by a wire mesh, we have N space basis functions including basis functions associated with junction nodes, M time functions, and $P = M \times N$ unknowns in the MOM scheme. The induced current is calculated for each unknown by solving (1) as described in the following.

Considering the Galerkin testing procedure, we use the functions defined in (6) for time variable and (7) for space variables, respectively. Defining

$$< f_m(t)g_n(\boldsymbol{r})\hat{s}, f_p(t)g_q(\boldsymbol{r}')\hat{s}' >$$
$$= \int_t \int_\ell f_m(t)f_p(t)g_n(\boldsymbol{r})g_q(\boldsymbol{r}')\,\hat{s}\cdot\hat{s}'\; d\ell\, dt \tag{8}$$

we can write (1) after testing as

$$< f_m(t)g_n(\boldsymbol{r})\hat{s}, \left[\frac{\partial^2 \boldsymbol{A}}{\partial t^2} + \nabla\Psi\right] >$$
$$= < f_m(t)g_n(\boldsymbol{r})\hat{s}, \left[\frac{\partial \boldsymbol{E}^i}{\partial t}\right] > \tag{9}$$

for $m = 1, 2, \ldots M$ and $n = 1, 2, \ldots N$.

Considering the integration on space variable, we can rewrite (9) as

$$\ell_n \int_t f_m(t)\left[\frac{\partial^2 \boldsymbol{A}(t,\boldsymbol{r}_n,\boldsymbol{r}')}{\partial t^2} \cdot \hat{s}_n\right]\, dt$$
$$+ \int_t f_m(t)\left[\Psi(t,\boldsymbol{r}_{n-\frac{1}{2}},\boldsymbol{r}') - \Psi(t,\boldsymbol{r}_{n+\frac{1}{2}},\boldsymbol{r}')\right]\, dt$$
$$= \ell_n \int_t f_m(t)\left[\frac{\partial \boldsymbol{E}^i(t,\boldsymbol{r}_n)}{\partial t} \cdot \hat{s}_n\right]\, dt \tag{10}$$

where $\hat{s}_n$ and ℓ_n represent the unit tangential vector at $\boldsymbol{r} = \boldsymbol{r}_n$ and length of the nth-wire segment, respectively [1].

Next, the integration on the time variable is carried out in the following manner:

1) Divide the interval $0 \to T$ into K uniform time intervals given by Δt_k and denote $t_k = (k-1)\Delta t_k + 0.5\Delta t_k$ for $k = 0, 1, 2, \ldots K$. Note that, in general, $\Delta t_k \neq \Delta t$ which also implies that $K \neq M$. However, for simplicity, we may choose them to be same.

2) Applying the numerical integration on time variable and using finite difference approximation, we can rewrite (10)

as

$$\frac{\ell_n}{\Delta t_k} \sum_{k=1}^K f_m(t_k)\, [\boldsymbol{A}(t_k,\boldsymbol{r}_n,\boldsymbol{r}')\cdot\hat{s}_n]$$

$$- \frac{2\ell_n}{\Delta t_k} \sum_{k=1}^K f_m(t_k)\, [\boldsymbol{A}(t_{k-1},\boldsymbol{r}_n,\boldsymbol{r}')\cdot\hat{s}_n]$$

$$+ \frac{\ell_n}{\Delta t_k} \sum_{k=1}^K f_m(t_k)\, [\boldsymbol{A}(t_{k-2},\boldsymbol{r}_n,\boldsymbol{r}')\cdot\hat{s}_n]$$

$$+ \sum_{k=1}^K f_m(t_k)\, \Psi(t_k,\boldsymbol{r}_{n-\frac{1}{2}},\boldsymbol{r}')\Delta t_k$$

$$- \sum_{k=1}^K f_m(t_k)\, \Psi(t_k,\boldsymbol{r}_{n+\frac{1}{2}},\boldsymbol{r}')\Delta t_k$$

$$= \ell_n \sum_{k=1}^K f_m(t_k)\, \left[\frac{\partial \boldsymbol{E}^i(t_k,\boldsymbol{r}_n)}{\partial t}\cdot\hat{s}_n\right]\Delta t_k. \tag{11}$$

Considering the expansion procedure next, we have

$$\boldsymbol{A}(t_k,\boldsymbol{r}_n,\boldsymbol{r}') = \mu \sum_{i=1}^M \sum_{j=1}^N I_{i,j}\, f_i\left(t_k - \frac{R_{n,j}}{c}\right)\hat{s}_j\,\kappa_{n,j} \tag{12}$$

for $k = 1, 2, \ldots, K$, where

$$\kappa_{n,j} = \int_{\ell_j} \frac{d\ell'}{4\pi\, R_n} \tag{13}$$

$R_n = |\boldsymbol{r}_n - \boldsymbol{r}'|$, $R_{n,j} = |\boldsymbol{r}_n - \boldsymbol{r}_j|$, and $\hat{s}_j$ is the unit tangential vector at $\ell = \ell_j$.

Next, let us consider the evaluation of $\Psi(t_k,\boldsymbol{r}_n,\boldsymbol{r}')$. Considering (3), replacing the derivative operation with finite difference approximation, and substituting (5), we have

$$\Psi(t_k,\boldsymbol{r}_n,\boldsymbol{r}') = \frac{-1}{\epsilon} \sum_{i=1}^M \sum_{j=1}^N I_{i,j}\, \frac{1}{\left|\ell_{j+\frac{1}{2}} - \ell_{j-\frac{1}{2}}\right|}$$
$$\times \left[f_i\left(\tau_{k,n,j+\frac{1}{2}}\right)\kappa_{n,j+\frac{1}{2}} - f_i\left(\tau_{k,n,j-\frac{1}{2}}\right)\kappa_{n,j-\frac{1}{2}}\right] \tag{14}$$

for $k = 1, 2, \ldots, K$ where

$$\kappa_{n,j\pm\frac{1}{2}} = \int_{\ell_{j\pm\frac{1}{2}}} \frac{d\ell'}{4\pi\, R_{n,j\pm\frac{1}{2}}}, \tag{15}$$

$$R_{n,j\pm\frac{1}{2}} = \left|\boldsymbol{r}_n - \boldsymbol{r}_{j\pm\frac{1}{2}}\right| \tag{16}$$

$$\tau_{k,n,j\pm\frac{1}{2}} = t_k - \frac{R_{n,j\pm\frac{1}{2}}}{c}. \tag{17}$$

Using the expansion and testing procedures described so far, it is trivial to generate a matrix equation $\boldsymbol{Z}\boldsymbol{X} = \boldsymbol{Y}$ of dimension $P = M \times N$. The elements of $\boldsymbol{Z}$-matrix are formed by using (11), (12), and (14). Note that $Z_{p,q}$ represents a matrix element of the $\boldsymbol{Z}$-matrix, where

$$p = (m-1)N + n, \quad q = (i-1)N + j$$
$$m, i = 1, 2, \ldots, M, \quad n, j = 1, 2, \ldots, N.$$

Thus, we have

$$
\begin{aligned}
Z_{p,q} = {} & \frac{\mu \ell_n}{\Delta t_k} \left[\hat{s}_n \cdot \hat{s}_j \; \kappa_{n,j}\right] \\
& \times \sum_{k=1}^{K} f_m(t_k) \left[f_i(\tau_{k,n,j}) - 2 f_i(\tau_{k-1,n,j}) + f_i(\tau_{k-2,n,j})\right] \\
& + \frac{\Delta t_k}{\epsilon \left|\ell_{j+\frac{1}{2}} - \ell_{j-\frac{1}{2}}\right|} \sum_{k=1}^{K} f_m(t_k) f_i\left(\tau_{k,n+\frac{1}{2},j+\frac{1}{2}}\right) \kappa_{n+\frac{1}{2},j+\frac{1}{2}} \\
& - \frac{\Delta t_k}{\epsilon \left|\ell_{j+\frac{1}{2}} - \ell_{j-\frac{1}{2}}\right|} \sum_{k=1}^{K} f_m(t_k) f_i\left(\tau_{k,n-\frac{1}{2},j+\frac{1}{2}}\right) \kappa_{n-\frac{1}{2},j+\frac{1}{2}} \\
& - \frac{\Delta t_k}{\epsilon \left|\ell_{j+\frac{1}{2}} - \ell_{j-\frac{1}{2}}\right|} \sum_{k=1}^{K} f_m(t_k) f_i\left(\tau_{k,n+\frac{1}{2},j-\frac{1}{2}}\right) \kappa_{n+\frac{1}{2},j-\frac{1}{2}} \\
& + \frac{\Delta t_k}{\epsilon \left|\ell_{j+\frac{1}{2}} - \ell_{j-\frac{1}{2}}\right|} \sum_{k=1}^{K} f_m(t_k) f_i\left(\tau_{k,n-\frac{1}{2},j-\frac{1}{2}}\right) \kappa_{n-\frac{1}{2},j-\frac{1}{2}}.
\end{aligned}
\tag{18}
$$

The right-hand side Y involves the incident field terms given by

$$
Y = [Y_1, Y_2, Y_3, \ldots, Y_M]^T \tag{19}
$$

where each Y_m, $m = 1, 2, \ldots M$ is a column vector of dimension N and the elements are given by

$$
(Y_n)_m = \ell_n \sum_{k=1}^{K} f_m(t_k) \left[\frac{\partial E^i(t_k, r_n)}{\partial t} \cdot \hat{s}_n\right] \Delta t_k. \tag{20}
$$

At this stage, we note that multiple incident pulses with varying frequency content can be easily accommodated by adding more column blocks to the Y-matrix.

As mentioned earlier, the choice of σ defined in (6) is important for the generation of a block Toeplitz matrix. Considering (6) and with the choice of $\sigma = \frac{\Delta t}{6}$, we observe that the mth-Gaussian function is essentially nonzero only in the interval $t = (m-1)\Delta t$ to $t = (m+1)\Delta t$. Here, we note the following.

1) Because of the nature of the retarded kernel, the matrix generated is a lower triangular matrix given by

$$
Z = \begin{bmatrix}
Z_{1,1} & \varnothing & \varnothing & \cdots & \varnothing \\
Z_{2,1} & Z_{2,2} & \varnothing & \cdots & \varnothing \\
Z_{3,1} & Z_{3,2} & Z_{3,3} & \cdots & \varnothing \\
\vdots & \vdots & \vdots & \vdots & \vdots \\
Z_{M,1} & Z_{M,2} & Z_{M,3} & \cdots & Z_{M,M}
\end{bmatrix} \tag{21}
$$

where each $Z_{m,i}$, $m = 1, 2, \ldots M$ and $i = 1, 2, \ldots, M$ is a matrix of dimension N representing the mutual interaction between the spatial basis functions for a given pair of testing time function m and source time function i.

2) Referring to (18), we note that for $i > m$, the matrix blocks are zero. This is because, for time functions $f_m(t_k)$ and $f_i(\tau_{k,n,j})$, the time intervals do not overlap resulting in zero value of the product.

3) We further note that all the diagonal blocks are the same and all off-diagonal blocks are given by $Z_{m,i} = Z_{|m-i|+1,1}$.

4) Because of the Toeplitz nature, only the blocks in the first column of (21) need to be computed and stored. All other blocks can be generated from the first column as needed.

5) Because of the lower triangular nature of the matrix, the solution can be obtained in a trivial manner. To obtain the solution, we need to invert and store the first block $Z_{1,1}$. However, this needs to be done only once.

Further, the response to next M time steps, i.e., from $T \to 2T$ can be easily obtained by only modifying the right-hand side. We note that for this case, the right-hand side would be $Y - \overline{Z} X_{\text{pre}}$, where X_{pre} represents the coefficients already calculated for zero to M-steps and $\overline{Z}$ represents the matrix containing vector and scalar potential terms contributing to zero to M time steps. The $\overline{Z}$-matrix is also Toeplitz and can be obtained in the same manner as Z-matrix. Also note that the $\overline{Z}$-matrix need not be inverted and may be stored if several M-time steps are needed.

IV. NUMERICAL RESULTS

In this section, we present numerical results for several conducting objects modeled by wire-grid with wire radius set equal to 0.001 m. Further, for all examples, the incident field is given by

$$
E^i(t, r) = E_o \frac{4}{T_P \sqrt{\pi}} e^{-\gamma^2} \tag{22}
$$

where

$$
\gamma = \frac{4}{T_P}(ct - ct_o - r \cdot a_k). \tag{23}
$$

In (22) and (23), a_k is the unit vector in the direction of propagation of the incident wave, T_P is the pulsewidth of the Gaussian impulse, $E_o \cdot a_k = 0$, r is a position vector relative to the origin, c is the velocity of propagation in the external medium, and t_o is a time delay which represents the time at which the pulse peaks at the origin. Also, we have $E_o = 120 \pi a_x$, $ct_0 = 6.0$ LM, $T - P = 4.0$ LM, and $k = -a_z$. Note that 1 LM = 3.333 ns. Further, for all examples, we have $T = 2 * ct_0 = 12$ LM, by which time the incident pulse drops to negligible value. Finally, we note that the number of time basis functions depend on the maximum frequency content of the incident pulse and 30–60 time-shifted Gaussian functions are required for the given incident field to generate reasonable accuracy in the time-domain solution.

Initially, we consider the same examples presented in [21] for comparison purposes and also to show that the present method is more efficient. The time history is restricted to 30 LM in each case to obtain proper measure of the efficiency.

As a first example, consider three straight wires, each 2.0 m long, placed along the x-, y-, and z-axes and joined at the origin, as shown in Fig. 3. Each wire is divided into ten segments and the wire-junction is illuminated by a Gaussian plane wave described by (22). The induced current at the center of the wire placed along the x-axis is obtained using the present procedure and shown in Fig. 3. The result is compared with [21]. There are 30 basis functions for space and time variables, respectively, for
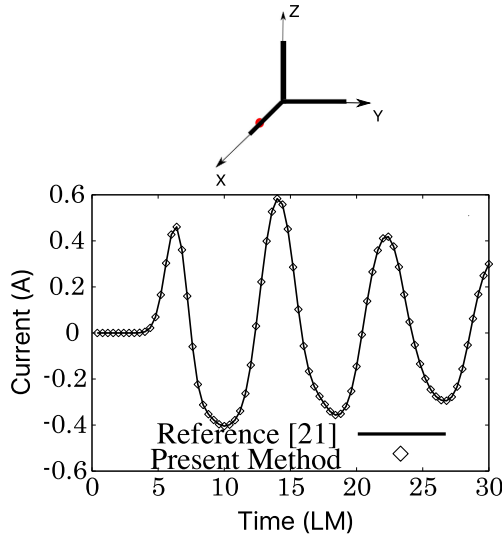
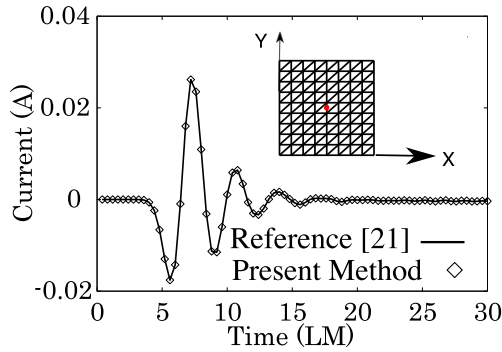Fig. 3. Current induced on a 3-wire structure illuminated by a Gaussian plane wave. The wire radius = 0.001 m.

Fig. 4. Current induced on a wire-mesh model of a square plate illuminated by a Gaussian plane wave. The wire radius = 0.001 m.
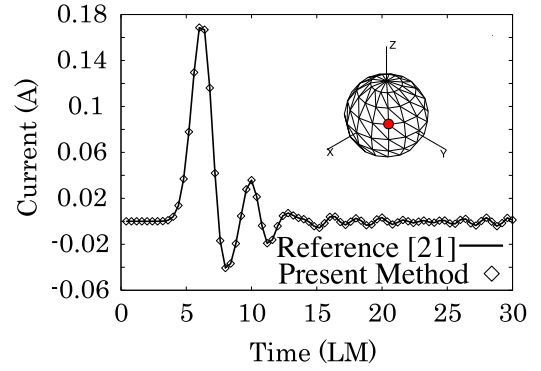

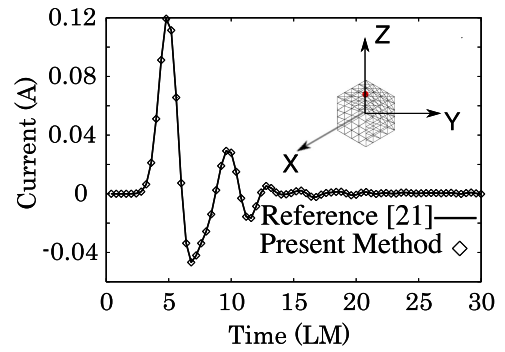Fig. 5. Current induced on a wire-mesh model of a sphere illuminated by a Gaussian plane wave. The wire radius = 0.001 m.

Fig. 6. Current induced on a wire-mesh model of a cube illuminated by a Gaussian plane wave. The wire radius = 0.001 m.

the time-domain solution. The CPU times for this problem are: 0.024 s for the present method and 3.964 s for [21].

Next, consider a wire-mesh arranged in the shape of a square plate of 1.0×1.0 m, located in the XY-plane. The mesh is illuminated by a Gaussian plane wave described by (22). The induced current at the center of the mesh, highlighted by a dot in the inset of Fig. 4, is obtained using the new procedure and compared with [21]. There are 377 and 30 basis functions for space and time variables, respectively, for both time-domain solutions. Both TD solutions compare very well, as shown in Fig. 4. The CPU times for this problem are: 7.452 s for the present method and 2126.2 s for [21].

Next, we consider a spherical wire-cage, 1.0 m radius, located with the center of the wire cage coinciding with the coordinate center. The mesh is illuminated by a Gaussian plane wave described by (22). The induced current is obtained at the equator of the sphere, highlighted by a dot in the inset of Fig. 5 using the TD solution procedure and compared with the IDFT solution. There are 449 and 30 basis functions for space and time variables, respectively, for both time-domain solutions. Both TD solutions compare very well, as shown in Fig. 5. The CPU times for this problem are: 9.68 s for the present method and 3813.2 s for [21].

As a fourth example, we consider a cubical wire-cage, 1.0 m side. The mesh is illuminated by a Gaussian plane wave described by (22). The induced current is obtained at the center of the top surface using the TD solution procedures of [21] and present procedure. There are 469 and 30 basis functions for space and time variables, respectively, for the time-domain solution. The numerical results for the present method and [21] are shown in Fig. 6, and compared very well. The CPU time for this problem are: 13.8 s for the present method and 4174.2 s for [21].

Now, we consider a few more examples using only the present procedure and compare the results with frequency domain solution combined with inverse discrete Fourier transform (IDFT) method.

Consider a conducting object shaped as an almond as shown in the inset of Fig. 7. We note that this is an object with a low radar cross section, and hence difficult to model. The object is described mathematically as follows:

Let (s, t) represent two parametric coordinates. Then, for the upper surface, we have $-\frac{5}{12} < t < 0$, $x = Lt$, $y = 0.193333L\sqrt{1-(\frac{12t}{5})^2}\cos s$, and $z = 0.064444L\sqrt{1-(\frac{12t}{5})^2}\sin s$. For the lower surface, we have $-\frac{25}{12} < t < 0$, $x = Lt$, $y = 4.83345L[\sqrt{1-(\frac{12t}{25})^2}-0.96]\cos s$, and $z = 1.61115L[\sqrt{1-(\frac{12t}{25})^2}-0.96]\sin s$. Also, the parameter s changes from $-\pi$ to π and $L = 1.4538$ m. The induced current is sampled at the center of the upper surface indicated by a dot in the figure. There are 1079 and 60 basis functions for space and time variables, respectively. The TD solution procedure is compared with
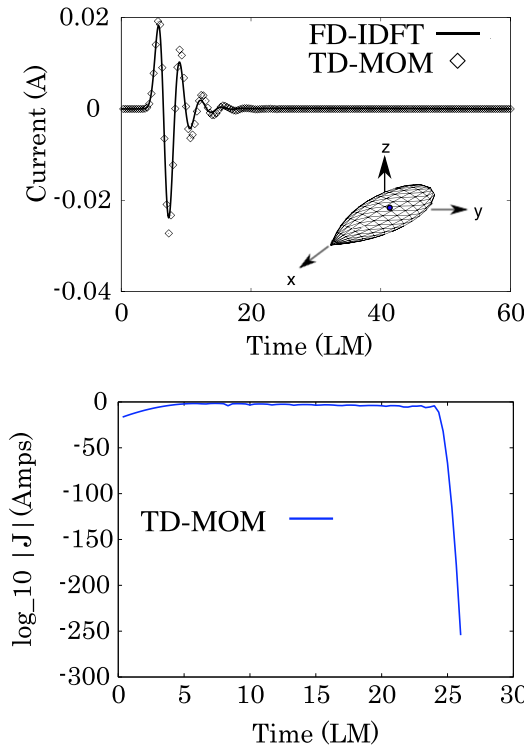
Fig. 7. Current induced on a wire-mesh model of an almond illuminated by a Gaussian plane wave. The wire radius =0.001 m.
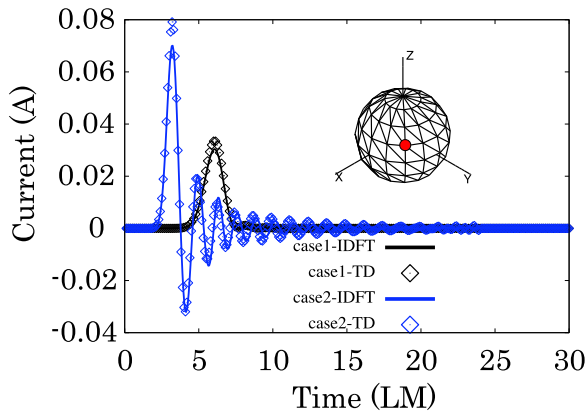

Fig. 8. Current induced on a wire-mesh model of a sphere of 0.5 m radius illuminated by a Gaussian plane wave. The wire radius = 0.001 m.

the IDFT solution. The IDFT solution is obtained by solving the frequency domain MOM problem at 256 equally spaced frequency points in the 0–400-MHz frequency band and performing the inverse Fourier transform. We note a good comparison between the two solutions.

To illustrate the absence of late time instabilities, the magnitude of the current is plotted as a function of time using log scale and shown in the same figure. Note that the base of the logarithm is 10. We note that the current reaches a value of 10^{-300} at around 25 LM and set to zero beyond.

Next, consider a sphere of 0.5 m radius, with center coinciding with the coordinate origin, modeled by thin wires, as shown in the inset of Fig. 8. This example is presented to illustrate the capability of the present method to handle multiple incident fields. The object is illuminated: 1) by a Gaussian impulse as in
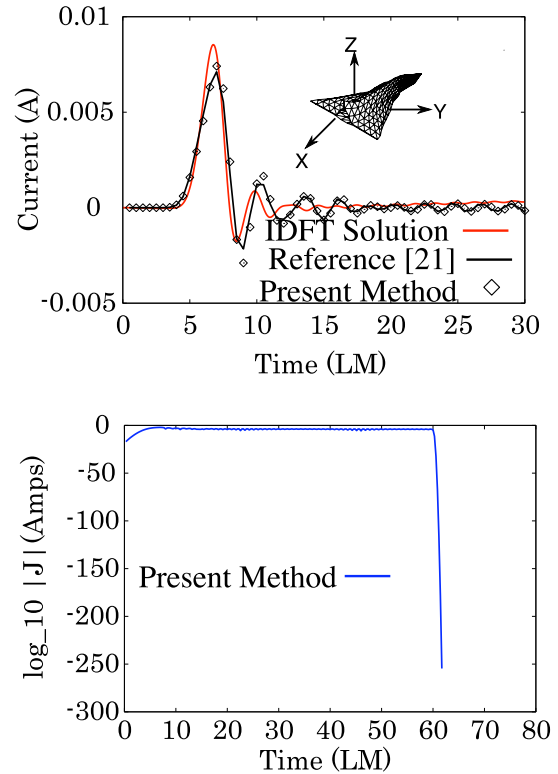

Fig. 9. Current induced on a wire-mesh model of an aircraft-like object illuminated by a Gaussian plane wave. The wire radius = 0.001 m.

the previous example (case 1), and 2) by a similarly polarized pulse with half the pulse width (case 2). The time-domain solution results are compared with the IDFT solution and presented in the Fig. 8. There are 524 and 60 basis functions for space and time variables, respectively. We note good comparison for both cases.

Next, we consider an aircraft-like object, as shown in Fig. 1. The object is symmetrically placed in the XY-plane such that the center of the lower side (belly) approximately coincides with the coordinate origin. The object dimensions are: 0.97 m, 0.86 m, and 0.25 m along the X-, Y-, and Z-axes, respectively. There are 1700 and 30 basis functions for space and time variables, respectively, for the time-domain solution. The current is sampled at the middle of an edge shown by a dot in the Fig. 1. The IDFT solution is obtained in a similar manner as in the previous example. The results obtained by FD-IDFT, [21], and the present method are shown in Fig. 9. Although there is a good comparison for all solutions, some discrepancies are apparent. These discrepancies may be attributed to possible insufficient sampling at the higher frequencies for the IDFT solution and may be corrected by a denser grid. However, we did not attempt developing a denser grid since it involves considerable effort. The CPU times for this problem are: 452.89 s, 4834.7 s, and 173,750 s for the present method, IDFT method, and [21], respectively.

Also, as in the case of almond, the magnitude of the current is plotted as a function of time using log scale and shown in the same figure. Note that the base of the logarithm is 10. We note that the current reaches a value of 10^{-300} at around 60 LM and set to zero beyond.
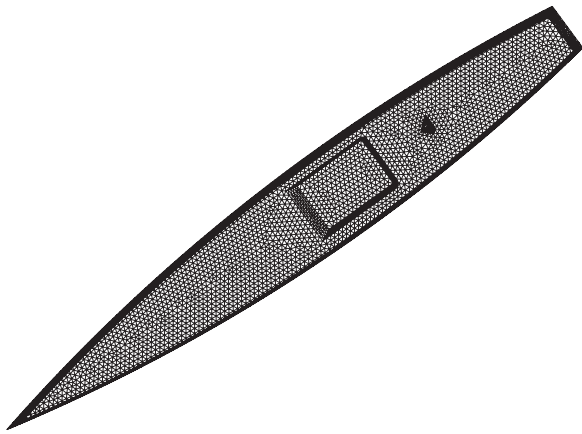
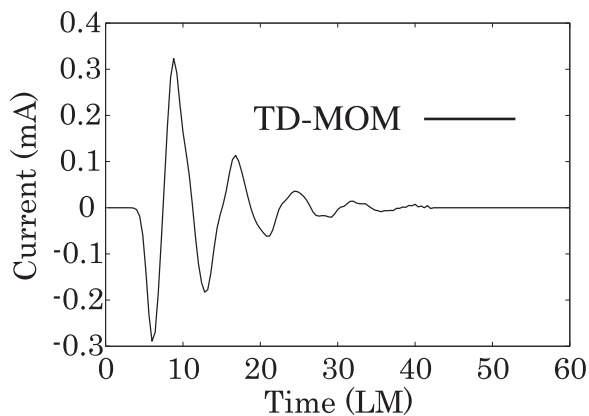Fig. 10.   Wire-grid model of a ship-like object.

Fig. 11.   Current induced on a wire-mesh model of a ship-like object illuminated by a Gaussian plane wave. The ship is 5.56 m long, 0.716 m wide, and 0.387 m height and placed such that the origin is approximately coinciding with center of the top deck. The wire radius = 0.001 m.

Finally, we consider a ship-like object, shown in Fig. 10. The ship is 5.56 m long, 0.716 m wide, and 0.387 m height and placed such that the origin is approximately coinciding with center of the top deck. There are 22 694 and 30 basis functions for space and time variables, respectively, for the time-domain solution. The current is sampled at the middle of the upper-deck approximately coinciding with $x = y = 0$. The numerical results obtained by the method presented in this paper is shown in Fig. 11. Also, note that IDFT solution for this example is prohibitively expensive and hence not attempted.

V. CONCLUSION

In this paper, a stable procedure is to solve the TDIE for conducting bodies using MOM solution procedure is presented. Note that the MOM matrix generated in this procedure is lower triangular and blockwise Toeplitz. Hence, solution of this matrix is extremely efficient.

ACKNOWLEDGMENT

REFERENCES

[1] S. M. Rao, *Time Domain Electromagnetics*. New York, NY, USA: Academic, 1999.
[2] D. A. Vechinski and S. M. Rao, "A stable procedure to calculate the transient scattering by conducting surfaces of arbitrary shape," *IEEE Trans. Antennas Propag.*, vol. 40, no. 6, pp. 661–665, Jun. 1992.
[3] A. Sadigh and E. Arvas, "Treating the instabilities in marching-on-in-time method from a different perspective," *IEEE Trans. Antennas Propag.*, vol. 41, no. 12, pp. 1695–1702, Dec. 1993.
[4] A. J. Pray, N. V. Nair, and B. Shanker, "Stability properties of the time domain electric field integral equation using a separable approximation for the convolution with the retarded potential," *IEEE Trans. Antennas Propag.*, vol. 60, no. 8, pp. 3772–3781, Aug. 2012.
[5] S. M. Rao, D. A. Vechinski, and T. K. Sarkar, "Transient scattering by conducting cylinders—Implicit solution for transverse electric case," *Microw. Opt. Technol. Lett.*, vol. 21, pp. 129–134, Apr. 1999.
[6] S. M. Rao and T. K. Sarkar, "Implicit solution of time domain integral equations for arbitrarily shaped dielectric bodies," *Microw. Opt. Technol. Lett.*, vol. 21, pp. 201–205, May 1999.
[7] S. M. Rao and T. K. Sarkar, "Numerical solution of time domain integral equations for arbitrarily shaped conductor/dielectric composite bodies," *IEEE Trans. Antennas Propag.*, vol. 50, no. 12, pp. 1831–1837, Dec. 2002.
[8] Jin-Lin Hu, C. H. Chan, and Yuan Xu, "A new temporal basis function for the time-domain integral equation method," *IEEE Microw. Wireless Compon. Lett.*, vol. 11, no. 11, pp. 465–466, Nov. 2001.
[9] Y. Beghein, K. Cools, H. Bagci, and D. De Zutter, "A space-time mixed Galerkin marching-on-in-time sScheme for the time-domain combined field integral equation," *IEEE Trans. Antennas Propag.*, vol. 61, no. 3, pp. 1228–1238, Mar. 2013.
[10] B. P. Rynne, "Stability and convergence of time marching methods in scattering problems," *IMA J. Appl. Math.*, vol. 35, no. 3, pp. 297–310, Nov. 1985.
[11] B.P. Rynne and P. D. Smith, "Stability of time marching algorithms for the electric field integral equation," *J. Electromagn. Waves Appl.*, vol. 4, no. 12, pp. 1181–1205, 1980.
[12] D. S. Weile, G. Pisharody, Nan-Wei Chen, B. Shanker, and E. Michielssen, "A novel scheme for the solution of the time-domain integral equations of electromagnetics," *IEEE Trans. Antennas Propag.*, vol. 52, no. 1, pp. 283–295, Jan. 2004.
[13] G. H. Zhang, M. Xia, and X.-M. Jiang, "Transient analysis of wire structures using time domain integral equation method with exact matrix elements," *Prog. Electromagn. Res.*, vol. 45, pp. 281–298, 2009.
[14] Y. Shi, M. Xia, R. Chen, E. Michielssen, and M. Lu, "Stable electric field TDIE solvers via quasi-exact evaluation of MOT matrix elements," *IEEE Trans. Antennas Propag.*, vol. 59, no. 2, pp. 574–585, Febr. 2011.
[15] H. A. Ulku and A. A. Ergin, "Application of analytical retarded-time potential expressions to the solution of time domain integral equations," *IEEE Trans. Antennas Propag.*, vol. 59, no. 11, pp. 4123–4131, Nov. 2011.
[16] B. H. Jung, Y. S. Chung, and T. K. Sarkar, "Time-domain EFIE, MFIE, and CFIE formulations using Laguerre polynomials as temporal basis functions for the analysis of transient scattering from arbitrarily shaped conducting structures," *Progr. Electromagn. Res.*, vol. 39, pp. 1–45, 2003.
[17] B. H. Jung, T. K. Sarkar, Y. S. Chung, M. Salazar-Palma, and Z. Ji, "Time-domain combined field integral equation using Laguerre polynomials as temporal basis functions," *Int. J. Numer. Model., Electron. Netw., Devices Fields*, vol. 17, pp. 251–268, 2004.
[18] Y. S. Chung *et al.*, "Solution of time domain electric field Integral equation using the Laguerre polynomials," *IEEE Trans. Antennas Propag.*, vol. 52, no. 9, pp. 2319–2328, Sep. 2004.
[19] Z. Ji, T. K. Sarkar, B. H. Jung, M. Yuan, and M. Salzar-Palma, "Solving time domain electric field integral equation without the time variable, "*IEEE Trans. Antennas Propag.*, vol. 54, no. 1, pp. 258–262, Jan. 2006.
[20] N. J. Sekljic, M. M. Ilic, and B. M. Notaros, "Spatially large and temporally entire-domain electric field integral equation method of moments for 3-D scattering analysis in time domain," *IEEE Trans. Antennas Propag.*, vol. 63, no. 6, pp. 2614–2626, Jun. 2015.
[21] S. M. Rao, "A stable marching-on-in-time algorithm capable of handling multiple excitations—Application to wire junction problems," *IET J. Microw., Antennas Propag.* vol. 12, no. 4, pp. 472–478, Mar. 2018.